Cardiovascular Pathology 22 (2013) 270–279

Contents lists available at SciVerse ScienceDirect

Cardiovascular Pathology

Original Article

Trypanosoma cruzi infection induces morphological reorganization of the myocardium parenchyma and stroma, and modifies the mechanical properties of atrial and ventricular cardiomyocytes in rats

Rômulo D. Novaes [a], Arlete R. Penitente [a], Reggiani V. Gonçalves [b], André Talvani [c], Maria C.G. Peluzio [d], Clóvis A. Neves [a], Antônio J. Natali [e], Izabel R.S.C. Maldonado [a,*]

[a] *Department of General Biology, Federal University of Viçosa, MG, 36570–000, Brazil*
[b] *Department of Morphology, Federal University of Juiz de Fora, MG, 36036–900, Brazil*
[c] *Department of Biological Sciences and NUPEB, Federal University of Ouro Preto, 35400–000, MG, Brazil*
[d] *Department of Nutrition and Health, Federal University of Viçosa, MG, 36570–000, Brazil*
[e] *Department of Physical Education, Federal University of Viçosa, MG, 36570–000, Brazil*

ARTICLE INFO

Article history:
Received 24 September 2012
Received in revised form 1 November 2012
Accepted 5 December 2012

Keywords:
Cardiac myocytes
Chagas' disease
Pathology
Extracellular matrix
Oxidative stress
X-ray spectroscopy

ABSTRACT

Background: This study investigates morphofunctional adaptations of the heart stroma and parenchyma in rats that are chronically infected with *Trypanosoma cruzi*.
Methods: Four-month-old male Wistar rats were randomized into control (n=14) and infected (n=14) groups. Infected animals were inoculated with *T. cruzi* Y strain. After 9 weeks, the animals were euthanized, and the right atrium (RA) and left ventricle (LV) were removed for biochemical, stereological, and cardiomyocyte mechanical analyses.
Results: Infected animals presented cardiomyocyte atrophy and myocardial fibrosis. For these animals, the total volume, length, surface area, and cross-sectional area of cardiomyocytes were significantly reduced, and the total interstitial and collagen volumes were significantly increased in the RA and LV compared to the controls. The total volume and length of blood vessels were significantly increased in the LV, and the total blood vessel surface area was significantly higher in the RA of infected animals. RA and LV cardiomyocytes from infected animals exhibited a significant reduction in cell shortening (43.02% and 24.98%, respectively), prolongation of the time to the peak of contraction (17.09%) and the time to half relaxation (23.68%) compared to non-infected animals. Lipid hydroperoxides, but not mineral concentrations, were significantly increased in the RA and LV from infected animals, showing an inverse correlation with cell shortening.
Conclusions: T. cruzi infection induces global structural remodeling of the RA and LV in rats. This remodeling coexists with cardiomyocyte contractility dysfunction, which is possibly related to the abnormal organization of the myocardial stroma and increased cellular lipid peroxidation.

1. Introduction

Chagas' disease (American trypanosomiasis) is caused by the hemoflagellate protozoan parasite *Trypanosoma cruzi*. This parasite infects nearly 10 million people worldwide and remains a leading cause of chronic heart failure in Central and South America [1] despite dramatic progress in transmission control [2]. Thousands of patients die every year, mainly due to dilated cardiomyopathy, congestive heart failure, dysrhythmias and thromboembolic events that occur in approximately 30% of infected subjects [3,4]. Owing to population migration, Chagas' disease also has the potential to become a health problem in non-endemic countries [2,5].

Although there is evidence that *T. cruzi* is able to spread and infect several organs, such as the gonads, kidney, liver, and pancreas in humans and animals, the cardiac form of the disease is the more severe and disabling [4,6]. Due to the intracellular parasite replication, differentiation, and cell evasion that occur during the acute phase of *T. cruzi* infection, the parasite triggers a destructive process in the myocardium. It has been suggested that this process is associated with an imbalance in the myocardial oxidative status, in which there is an increase in lipid and protein oxidation that causes progressive deterioration of the cardiomyocyte structure and function and, eventually, leads to cell death [7–10]. In parallel to myocardium destruction there is a reaction to repair the heart parenchyma and stroma, which reduces the progression of the cardiac lesions,

* Corresponding author. Department of Physical Education, Federal University of Viçosa, Av. Peter Henry Rolfs, s/nº, Zip code: 35.570-000. Viçosa-MG, Brasil. Tel.: +55 31 3899 4390; fax: +55 31 3899 2249.
E-mail address: irscosta@ufv.br (I.RSC. Maldonado).

1054-8807/$ – see front matter © 2013 Elsevier Inc. All rights reserved.
http://dx.doi.org/10.1016/j.carpath.2012.12.001

reducing the severity of the infection [4,11]. The heart failure observed in severe cases of the disease develops gradually during *T. cruzi* infection, when destructive events outweigh the reparative myocardial events [3,6].

During the transition from the acute to the chronic phase of *T. cruzi* infection, there is a progressive morphological and functional reorganization of the heart [2,6,12]. Traditionally, the evidence of myocardium structural remodeling induced by *T. cruzi* is mainly based on qualitative or semi-quantitative studies [11,13–15]. Moreover, most of the histo-quantitative data are described as relative values related to a two-dimensional reference space. To the best of our knowledge, the basic characteristics of the myocardial morphological reorganization in a three-dimensional space remain an unresolved issue in *T. cruzi* infection. Therefore, understanding the extent of cardiac damage in Chagas' cardiomyopathy (ChC) is essential for the design of rational intervention strategies.

In addition to the morphological remodeling of the heart in ChC, pathological changes in cardiac function are also commonly seen. Electrical changes of the sinus rhythm, conduction blocks of the action potential and atrial and ventricular arrhythmias have been widely described [3,11]. Moreover, mechanical and hemodynamic abnormalities, such as reduced end-diastolic volume, different strengths of muscle contractions, and altered heart rate and cardiac output, are also involved in cardiac dysfunction and contribute to the increased risk of death in *T. cruzi* infection [1,2,4,12]. However, the biochemical and cellular basis of ChC remains poorly understood.

Thus, this study used a stereological approach and cell isolation to investigate the morphofunctional adaptations of the heart stroma and parenchyma in the chronic phase of *T. cruzi* infection. Considering the relationship between cardiac structure and function, this study investigates the hypothesis that structural myocardial remodeling coexists with changes in oxidative status of the myocardium and pathological adaptations of the cardiomyocytes mechanical properties.

2. Methods

2.1. Animals and infection

Four-month-old male Wistar rats were provided with rodent chow and water ad libitum and maintained in animal facilities with a controlled environment (temperature at 22±3°C, humidity at 60–70% and 12-h light/dark inverted cycles). Animals were randomly divided into control (CG, $n=14$) and infected (IG, $n=14$) groups. Animals from the IG were inoculated intraperitoneally with the *T. cruzi* Y strain (300,000 trypomastigotes/50 g body weight) [16] contained in 700 μl of infected blood from a mouse that had been diluted in 0.9% saline solution. Infection was confirmed 4 days post-inoculation by the presence of trypomastigotes in peripheral blood collected from the rat's tail as described by Brener [17]. Nine weeks after inoculation, the animals were euthanized under anesthesia and the hearts were removed for stereological and contractile function analyses. All experimental procedures were conducted in accordance with the Brazilian College of Animal Experimentation and approved by the Animal Research Ethics Commission of the Federal University of Viçosa, Brazil (protocol 30/2009).

2.2. Sample size and tissue processing

The hearts from five animals per group were removed for stereological analysis. The sample size for this analysis was determined considering the probability $P=1/2$ to increase or decrease of the variables of interest. Thus, considering the significance level $\alpha=.05$, the minimal significant number of animals used in the statistical analysis was $P=(1/2)^{\text{events}}$; so, if $n=5$, $P=(1/2)^5$ or $P=.03$; thus, $P<.05$ [18].

The right atrium (RA) and the left ventricle (LV) were sampled randomly, dissected and the volumes were determined using the submersion method described by Scherle [19]. The LV volume was determined, including the inter-ventricular septum. The RA and LV were placed into histological fixative for 48 hours (freshly prepared 10% w/v formaldehyde in 0.1M phosphate buffer pH 7.2). The fragments of the RA and LV were obtained through the *orientador* method for stereological study [20]. These fragments were dehydrated in ethanol, cleared in xylol, and embedded in paraffin. Blocks were cut into 4-μm-thick histological sections stained with hematoxylin-eosin (H&E), 4′,6-diamidino-2-phenylindole (DAPI) and Phalloidin, and mounted on histology slides. To avoid repeated analysis of the same histological area, sections were evaluated in semi-series, using 1 out of every 20 sections. The slides were visualized and the images captured using a light microscope (Olympus BX-60, Tokyo, Japan) connected to a digital camera (Olympus QColor-3, Tokyo, Japan). Sections stained with DAPI and Phalloidin were visualized using the epifluorescence mode of the same microscope.

2.3. Tissue shrinkage

The processing of biological tissues for microscopy often leads to tissue shrinkage, especially when embedded in paraffin. In order to avoid false estimations of the absolute stereological parameters, tissue shrinkage was calculated. Two small tissue fragments with known volumes [19] from each animal were carefully embedded in paraffin. The embedded samples were totally cut with a microtome advance of 5μm and every 25th section was mounted on a histology slide. The tissue block volumes were microscopically determined using the Cavalieri's principle [21], and this volume was compared to the original volume of the tissue blocks before embedding. The global shrinkage of cardiac tissue was 21% and the stereological estimates were corrected using this index.

2.4. Estimation of absolute stereological parameters, cross-sectional area of cardiomyocytes and diffusion distance

All of the stereological analysis was performed according Brüel et al. [22]. The volume density occupied by cardiomyocytes (Vv [cmy], %), interstitium (Vv[int], %) and blood vessels (Vv[bvs], %) in the RA and LV were estimated by point counting according to the following formula:

$$\text{Vv}[structure/\text{RA};\text{LV}] = \frac{\sum P[structure]}{\sum Pt} \tag{1}$$

where ΣP[structure] is the number of points that hit the interest structure and ΣPt denotes the total test points. For these analyses, a test system of 42 points was used in an unbiased two-dimensional test area (At) of $1.38\times10^4\mu m^2$ at tissue level.

The length density of the cardiomyocytes (Lv[cmy], mm^{-2}) and blood vessels (Lv[bvs], mm^{-2}) in the RA and LV, were estimated as follows:

$$\text{Lv}[structure/\text{RA};\text{LV}] = 2\times\frac{\sum Q^{-}[structure]}{\sum P[RA;LV]}\times\frac{Pt}{At}; \tag{2}$$

where ΣQ^{-}[structure] denotes the total number of interest structure profiles counted in the At, and ΣP[RA; LV] is the total number of points hitting the RA and LV (the reference space) [22].

The surface area density of the cardiomyocytes (Sv[cmy], mm^{-1}) and blood vessels (Sv[bvs], mm^{-1}) in the RA and LV, were estimated using the following equation:

$$\text{Sv}[structure/\text{RA};\text{LV}] = 2\times\frac{\sum I[structure]}{\sum P[structure]}\times\frac{Pt}{l}; \tag{3}$$

where ΣI[structure] denotes the total number of intersections between the test lines (here 21) and the surface area of the structure of interest, and *l* is the length of a test line.

The total volume of cardiomyocytes (V[cmy], mm^3), interstitium (V[int], mm^3) and blood vessels (V[bvs], mm^3); the total length of cardiomyocytes (L[cmy], km) and blood vessels (L[bvs], km); and the total surface area of cardiomyocytes (S[cmy], m^2) and blood vessels (S[bvs], m^2) were estimated by multiplying the relative parameters of density by RA and LV volume.

The mean diffusion distance from capillary to tissue (r̂[bvs], μm^2), was obtained from equation 4:

$$\hat{r}[bvs/\mathrm{RA};\mathrm{LV}] = \sqrt{\frac{1}{\times \mathrm{Lv}[bvs]}}; \tag{4}$$

The mean cross-sectional area of cardiomyocytes (ā[cmy], μm^2) was calculated as follows:

$$\mathrm{a}[cmy] = \frac{\mathrm{Vv}[cmy]}{\mathrm{Lv}[cmy]}; \tag{5}$$

For all of these analyses, sixty microscopic fields (magnification ×400) in sections stained with H&E were randomly sampled and a total of 8.27×10^5 μm^2 of myocardium area was analyzed for each group.

2.5. Fibrosis and inflammation

Heart fibrosis was evaluated in 4μm-thick thick histological sections stained with Sirius red dye (Sirius red F3B; Mobay Chemical, Union, NJ, USA), which marks collagen fibers for observation under a polarizing microscope [23]. The distribution of collagen was analyzed using a segmentation function of the image analysis software Image Pro-Plus 4.5 (Media Cybernetics, Silver Spring, MD, USA) based on the birefringence properties of the collagen fibrils under polarized light. After image segmentation, the volume density (Vv[col], %) and total volume of the myocardium occupied by collagen fibers (V[col], μm^3) were determined using Eq. 1 and the RA and LV volumes. In this analysis, sixty microscopic fields were investigated (magnification ×200) by random sampling, and a total myocardium area of 3.34×10^6 μm^2 was analyzed for each group.

The intensity of heart inflammatory process was investigated in sections stained with H&E by the relationship between the mononuclear (MN) and polimorphonuclear (PMN) cell numbers observed in the myocardium from control and infected animals. The tissue cellularity was evaluated by counting the number of nuclei at ×1000 magnification across sixty random microscopic fields in a total myocardium area of $2.04\times10^5\mu m^2$ for each group [24]. Cardiomyocyte nuclei were excluded from this count. All morphological analysis was performed using the image analysis software Image Pro-Plus 4.5 (Media Cybernetcs, Silver Spring, MD, USA).

2.6. Cardiomyocytes isolation and contractile function

At euthanasia, the hearts of nine animals from each group were rapidly removed and the extraneous tissue was dissected away. The hearts were mounted onto a Langendorff perfusion apparatus for the isolation of myocytes using a collagenase-protease dispersion technique as previously described [25]. Briefly, the heart was perfused for 10–15 min with a solution containing 1mg/ml of collagenase type II (Worthington, USA). Ventricular and atrial cardiomyocyte cells were isolated by mechanical titration over 5 minutes at 37°C, with single cells separated from the non-dispersed tissue by filtration. Only calcium-tolerant, quiescent, rod-shaped cardiomyocytes showing clear cross striations were studied. The isolated cardiomyocytes were used within 4 h of isolation.

Cellular contractile function was evaluated as described by Natali et al. [25]. Briefly, isolated cells were placed in a chamber with a glass coverslip base mounted on the stage of an inverted-type phase contrast video microscope (Eclipse-TS100, Nikon, Japan). The chamber was perfused with Tyrode's solution at room temperature (≈28°C). Myocytes were stimulated via platinum bath electrodes with voltage pulses of 5ms duration and an intensity of 20V at 1 Hz. Cells were visualized on a PC monitor with an NTSC camera (Myo-Cam CCD100V, Ionoptix, Milton, MA, USA) set in scanning mode. This image was used to measure cell shortening (index of contractile function) in response to electrical stimulation, using a video motion edge detection system (Ionoptix, Milton, MA, USA). The cell image was sampled at 240Hz and cell shortening was calculated from the output of the edge detector using an IonWizard A/D converter (Ionoptix, Milton, MA, USA). Eight to 16 consecutive contractions were averaged and cell shortening (expressed as percentage of resting cell length), the time to the shortening peak, and the time to half-relaxation were calculated [26].

2.7. Mineral microanalysis and lipid peroxidation

The mineral content in heart tissue was investigated by Energy Dispersive X-ray Spectroscopy (EDS) using a scanning electron microscope (Leo 1430VP, Carl Zeiss, Jena, Thuringia, Germany) with an attached x-ray detector system (Tracor TN5502, Middleton, WI, USA). Small RA and LV pieces from each animal that had not been used for the stereological analysis were dissected, and three other fragments were obtained so that each one represented a different region of the myocardium: sub-epicardial, central and sub-endocardial. These fragments were dehydrated in ethanol, submitted to critical point drying (CPD 030, Bal-tec, Witten, North Rhine-Westphalia, Germany), and coated with a thin film of evaporated carbon (Quorum Q150 T, East Grinstead, West Sussex, England, UK). The EDS microanalysis was performed at ×800 magnification, with an accelerating voltage of 20 kV and a working distance of 19 mm. The proportion of the elements carbon (C), nitrogen (N), oxygen (O), potassium (K), phosphorus (P), sodium (Na), calcium (Ca), and magnesium (Mg) were measured by EDS and expressed as a mean value for all of the myocardium regions analyzed.

After enzymatic digestion, aliquots of the RA and LV from each heart used for cardiomyocyte isolation were homogenized in phosphate-buffered saline (PBS) and centrifuged at 5°C. The supernatant was used to determine the lipid hydroperoxide tissue levels using a standardized methodology [27]. Lipid hydroperoxide levels were normalized by the tissue content of total protein measured using the Bradford assay [28].

Table 1
Estimates of coefficients of variation for the stereological parameters

Parameter	Right atrium/left ventricle		
	*CV*tot	*CV*bio	*CE*met
V[cmy]	0.09/0.12	0.09/0.11	0.03/0.04
V[int]	0.17/0.12	0.16/0.11	0.05/0.04
V[bvs]	0.11/0.11	0.10/0.11	0.03/0.04
V[col]	0.19/0.17	0.18/0.17	0.06/0.06
L[cmy]	0.14/0.11	0.13/0.11	0.04/0.04
L[bvs]	0.12/0.08	0.11/0.08	0.04/0.03
S[cmy]	0.16/0.07	0.15/0.07	0.05/0.02
S[bvs]	0.19/0.14	0.19/0.13	0.06/0.04
r̂[bvs]	0.16/0.16	0.15/0.16	0.05/0.05
ā[cmy]	0.05/0.05	0.05/0.04	0.02/0.01

*CV*tot, total coefficient of variation; *CV*biol, biological coefficient of variation; *CE*met, coefficient of error of the stereological procedure.

2.8. Statistical analysis

Data are presented as means and standard deviations (mean± S.D). Normal distribution of data was verified using the Kolmogorov-Smirnov test. The coefficient of variation (CV) was calculated to investigate the homogeneity in the distribution of animal body mass. The observed total variation (CVtot) and the coefficient of error of the stereological procedure (CEmet) were estimated. From CVtot and CEmet, the biological variation (CVbio) was calculated as follows [22]: $CV\text{bio} = \sqrt{CV\text{tot}^2 - CE\text{bio}^2}$. The CE's from the various stereological estimators used are within acceptable limits (Table 1). Biometric, biochemical and cell

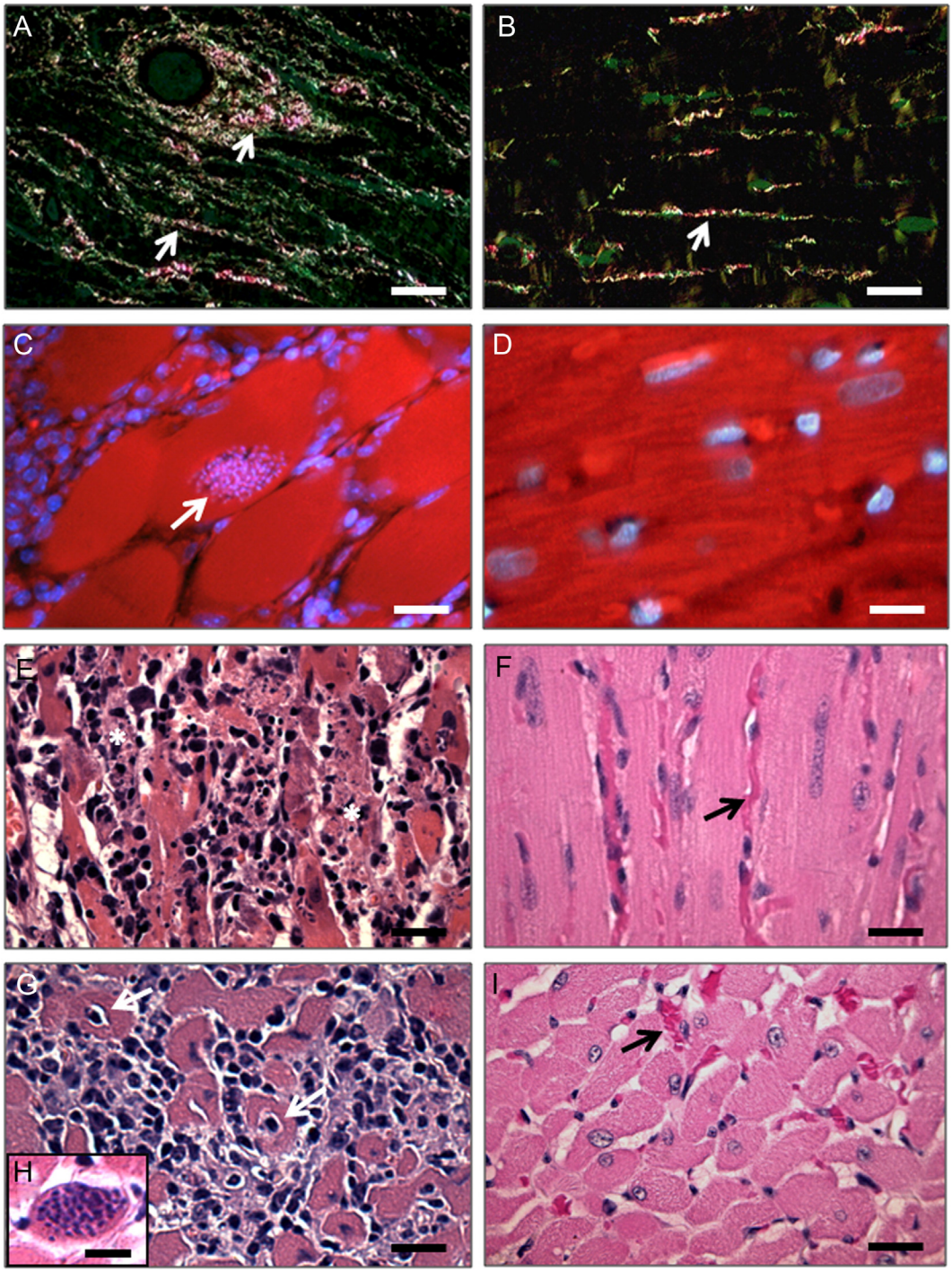

Fig. 1. Representative photomicrographs of the left ventricle from infected (A, C, E, G and H) and control (B, D, F, and I) rats. (A) Intense deposition of collagen fibers (arrows) with pericellular and perivascular distribution in the myocardium of infected animals (Sirius red staining under polarized light microscopy, bar=30 μm). (B) A lower density of collagen fibers is observed in the control group (Sirius red staining under polarized light microscopy, bar=30 μm). (E) Focal necrosis with cardiomyocytes fragmentation (asterisks) and intense leukocyte infiltration are observed in the myocardium of infected animals. In these animals a myocardial cross-section shows cardiomyocytes with reduced diameters, pyknotic nuclei (arrow) and diffuse inflammatory infiltrates (G) (H&E staining, bar=30 μm). Detail of an intracellular nest of *T. cruzi* is observed in (C) (DAPI and Phaloidin staining under epifluorescence microscopy, bar=20 μm) and (H) (H&E staining, bar=30 μm). For the control animals (D, F, and I) the myocardium showed a well-organized structure. Blood capillaries are indicated by the arrows (H&E staining, bar=30 μm).

Table 2
Stereological parameters and cellularity of the myocardium from control and infected rats

Parameter	Control	Infected
Right atrium		
V[col] (mm^3)	9.37±2.13	15.62±2.80*
V[bvs]/V[cmy]	0.14±0.01	0.18±0.02*
V[int]/V[cmy]	0.52±0.11	0.82±0.20*
ā[cmy] (μm^2)	52.20±8.84	36.36±5.12*
r̂[bvs] (μm^2)	5.45±0.27	5.29±0.31
MN cell (N/170×10^3 μm^2)	71.27±17.65	279.12±34.01*
PMN cell (N/170×10^3 μm^2)	29.86±16.05	77.25±18.85*
Left ventricle		
V[col] (mm^3)	29.56±5.40	49.67±8.16*
V[bvs]/V[cmy]	0.16±0.03	0.24±0.03*
V[int]/V[cmy]	0.43±0.07	0.81±0.19*
ā[cmy] (μm^2)	52.78±8.83	36.65±5.84*
r̂[bvs] (μm^2)	5.28±0.25	4.89±0.22*
MN cell (N/170×10^3 μm^2)	68.62±19.49	302.70±40.57*
PMN cell (N/170×10^3 μm^2)	25.47±14.51	172.92±17.36*

V, total volume; [col] collagen fibers; [bvs], blood vessels; [cmy], cardiomyocytes; [int], interstitium; ā[cmy], mean cross-sectional area of cardiomyocytes; [bvs], mean diffusion distance; MN, mononuclear cells; PMN, polymorphonuclear cells. The data are represented as mean±S.D.

* Denotes statistical difference from control for the same segment ($P<.001$), Student's *t* test.

contractile function data were compared using the student t-test. Stereological data were compared using the Mann–Whitney *U* test. A probability of $P<.05$ was considered statistically significant.

3. Results

3.1. Biometrical analysis

The initial (362.68±31.19 g; CV=0.09) and final (503.83±27.00 g; CV=0.05) body mass of the animals used in this study was similar in both groups, with no significant difference. There was also no significant difference between the RA volume in the CG (113.58±7.01 mm^3, CV=0.06) and IG (117.31±5.14 mm^3, CV=0.04) animals. The LV volume was significantly higher in IG animals (487.69±34.89 mm^3, CV=0.07) compared with CG animals (456.47±26.18 mm^3, CV=0.06).

3.2. Myocardial histopathology and stereology

Myocardial pathological changes were evident in the RA and LV after nine weeks of *T. cruzi* infection. Infected animals showed intracellular *T. cruzi* amastigote nests and intense diffuse inflammatory infiltrates with a predominance of mononuclear cells (Fig. 1). The density of mononuclear cells and polymorphonuclear cells was significantly higher in the RA and LV myocardium of IG animals compared to the CG animals (Table 2). For the IG animals, cellular atrophy was identified with cardiomyocytes showing pyknotic nuclei, intense and diffuse myocardial fibrosis and focal tissue necrosis. These characteristics were not observed in the CG animals (Fig. 1).

The IG animals presented a significant reduction of the total volume and the total length occupied by cardiomyocytes in the RA

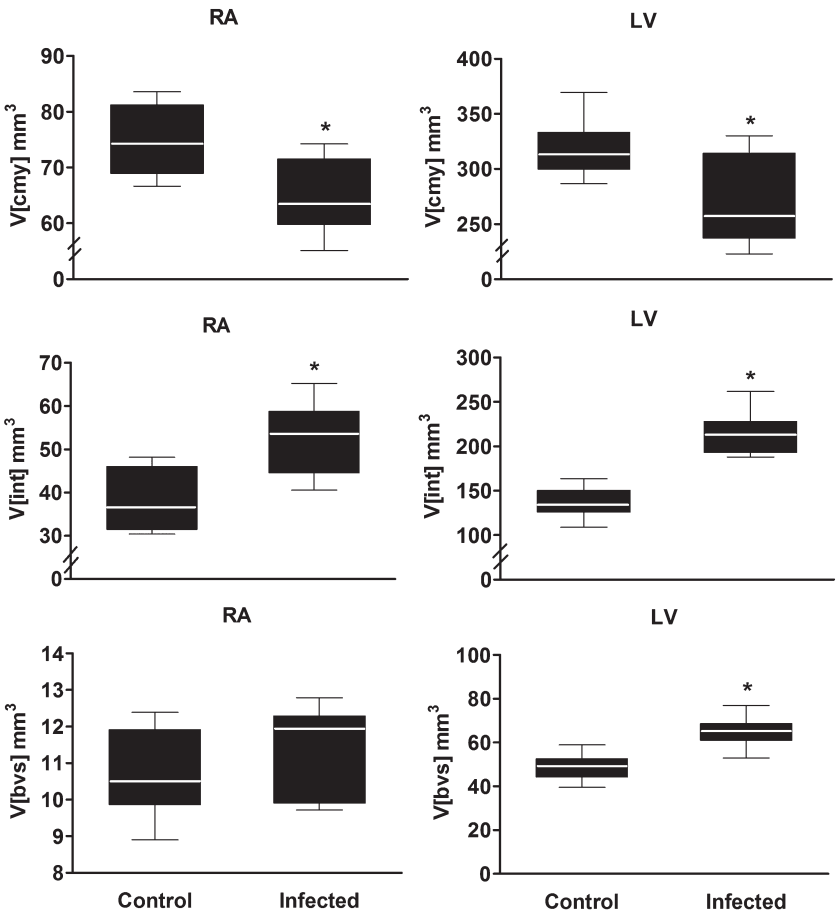

Fig. 2. Total volume occupied by cardiomyocytes (V[cmy]), interstitium (V[int]) and blood vessels (V[bvs]) in the RA and LV from control and infected rats. The box represents the interquartile interval with the median indicated (horizontal line), and whiskers represent the superior and inferior quartiles. *Denotes statistical difference from control ($P<.001$) for the same segment, Mann–Whitney *U* test.

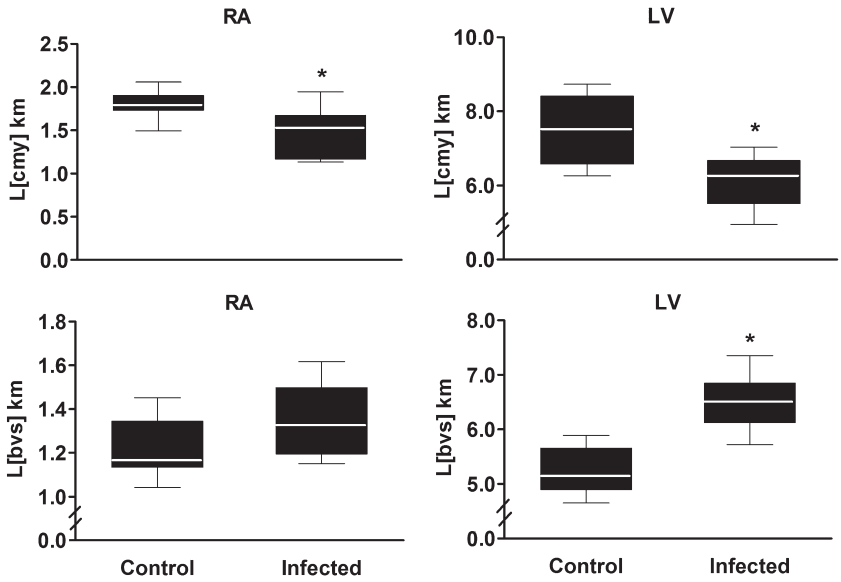

Fig. 3. Total length of cardiomyocytes (L[cmy]) and blood vessels (L[bvs]) in the RA and LV from control and infected rats. The box represents the interquartile interval with the median indicated (horizontal line), and whiskers represent the superior and inferior quartiles. *Denotes statistical difference from control ($P<.001$) for the same segment, Mann–Whitney *U* test.

and LV compared to the CG animals (Fig. 2). Conversely, the total interstitial volume and the total collagen volume were significantly increased in the RA and LV of IG animals (Table 2 and Fig. 2). The total volume and total length of blood vessels was significantly increased only in the LV of IG animals (Fig. 2 and 3).

Infected animals presented with a significant reduction of the total surface area and mean cross-sectional area of cardiomyocytes in the RA and LV and total blood vessel surface area in the RA compared to CG animals (Table 2 and Fig. 4). The total surface area of blood vessels was significantly higher in the LV of IG animals (Fig. 4). The mean diffusion distance from the capillary to tissue was similar for both groups (Table 2).

3.3. Cardiomyocyte contractility

The analysis of cell contractility showed marked changes in the mechanical properties of isolated cardiomyocytes from IG animals (Fig. 5). In this group, RA and LV cardiomyocytes presented with a significant reduction in cell shortening (43.02% and 24.98%, respectively) compared to the CG animals. The curve of cell contractility as a function of time showed a lower amplitude of variation of cell length in IG animals (Fig. 5). In addition, RA and LV cardiomyocytes had a significant prolongation of the time to the peak of contraction (17.09%) and the time to half relaxation (23.68%) in relation to the CG animals. These results are also indicated by a

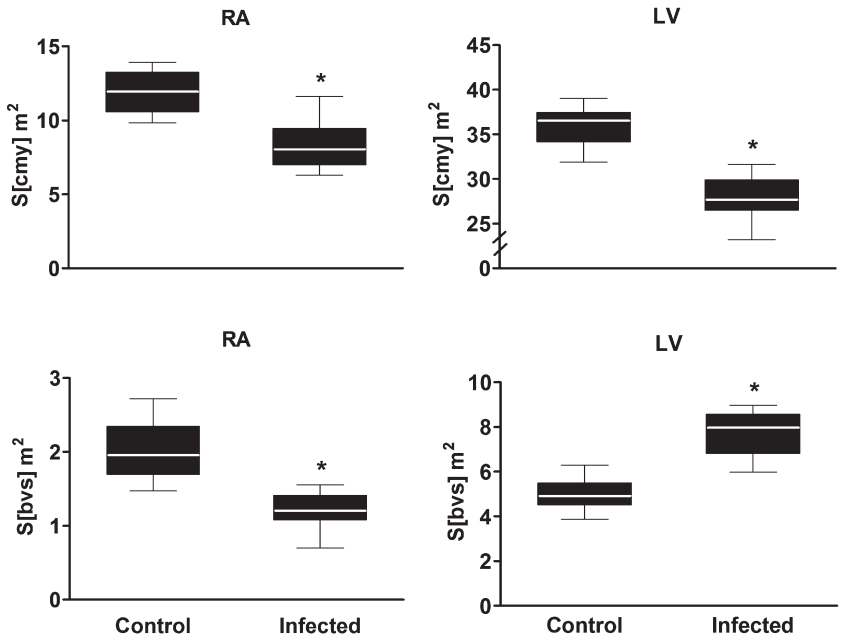

Fig. 4. Total surface area of cardiomyocytes (S[cmy]) and blood vessels (S[bvs]) in the RA and LV from control and infected rats. The box represents the interquartile interval with the median indicated (horizontal line), and whiskers represent the superior and inferior quartiles. *Denotes statistical difference from control ($P<.001$) for the same segment, Mann–Whitney *U* test.

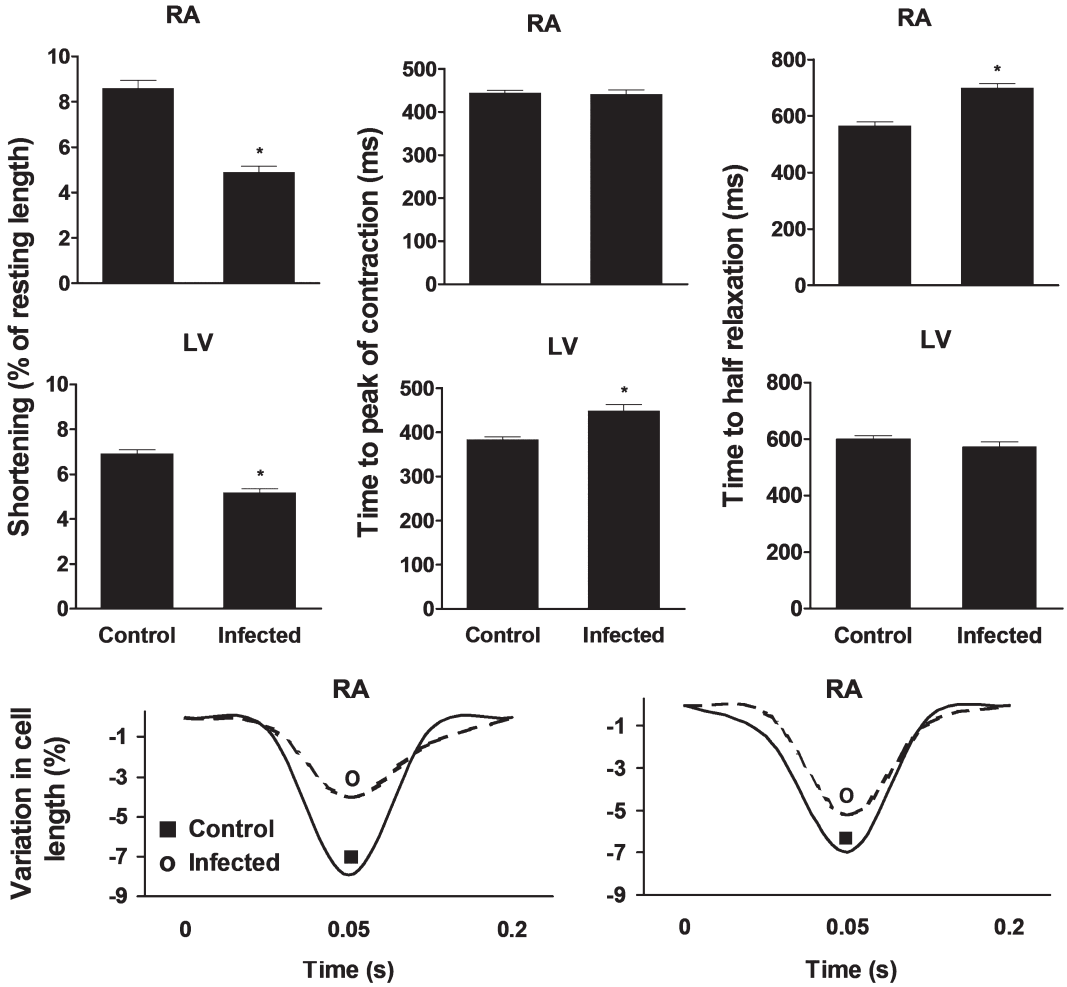

Fig. 5. Contractility parameters of cardiomyocytes of the RA and LV from control and infected rats. The data are represented as mean±S.D. *Denotes statistical difference from control ($P<.001$) for the same segment, Student's *t* test.

marked prolongation of the relaxation and contraction components in the curve of cell contractility relative to the RA and LV, respectively (Fig. 5).

3.4. Mineral microanalysis and lipid peroxidation

The mineral concentration in the RA and LV was similar in both groups investigated, with no statistical difference between them (Fig. 6). The biochemical analysis indicated a significant increase in lipid hydroperoxide (HPX) levels in the RA and LV from IG animals compared to the CG animals. The linear regression analysis showed a moderate and significant inverse correlation between the amplitude of cell shortening and the lipid HPX levels in the RA and LV from IG animals (Fig. 7). The correlation was not significant for CG animals.

4. Discussion

In the present study, infection was induced using a *T. cruzi* Y strain due to its high virulence and tropism by cardiac tissue [29,30]. The results showed that the standardized inoculum and the consequential *T. cruzi* infection were sufficient to stimulate lipid peroxidation, induce marked myocardial morphological reorganization and cardiomyocyte contractile dysfunction.

The present study showed that *T. cruzi* infection induced marked RA and LV structural remodeling. Using design-based stereology methods it was possible to identify for the first time that this remodeling extends beyond the focal or relative features considered pathognomonic of ChC, such as cell parasitism, mononuclear inflammatory infiltrate, microvascular constriction, fibrosis, cardiomyocitolysis, and necrosis [6,15,31]. Taken together, the stereological data indicated that the pathological reorganization of the myocardial stroma and parenchyma changes the global histoarchitecture of the RA and LV. Interestingly, although an evident reduction in total cardiomyocyte volume has been observed, the RA and LV volume were not reduced in IG animals. This finding clearly demonstrates the adaptability of the myocardial stroma in response to the parenchymal damage. Thus, the reactive expansion of the extracellular matrix components, especially through collagenogenesis and neoangiogenesis, represents important processes related to the cardiac remodeling in ChC, which is evident in the replacement of functional components by structural myocardial components [3,14,15].

Recently, studies conducted in our laboratory have clarified new aspects of the ChC pathogenesis [26,29,30]. These studies indicate for the first time that the deterioration of cardiac function observed in the acute and chronic phases of ChC represents a cellular basis related to cardiomyocyte mechanical insufficiency. In the present study, temporal and spatial evidence of contractile incompetence were observed in the cardiomyocytes that resisted infection. Interestingly, dysfunctional cardiomyocytes were isolated from infected RA and LV myocardium presenting a completely altered structural microenvironment. In fact, the myocardial volume occupied by cardiomyocytes was decreased and the extracellular matrix (ECM) volume (V[int]) was markedly increased in the RA and LV. However, the volume occupied by blood vessels was only increased in the LV. Moreover,

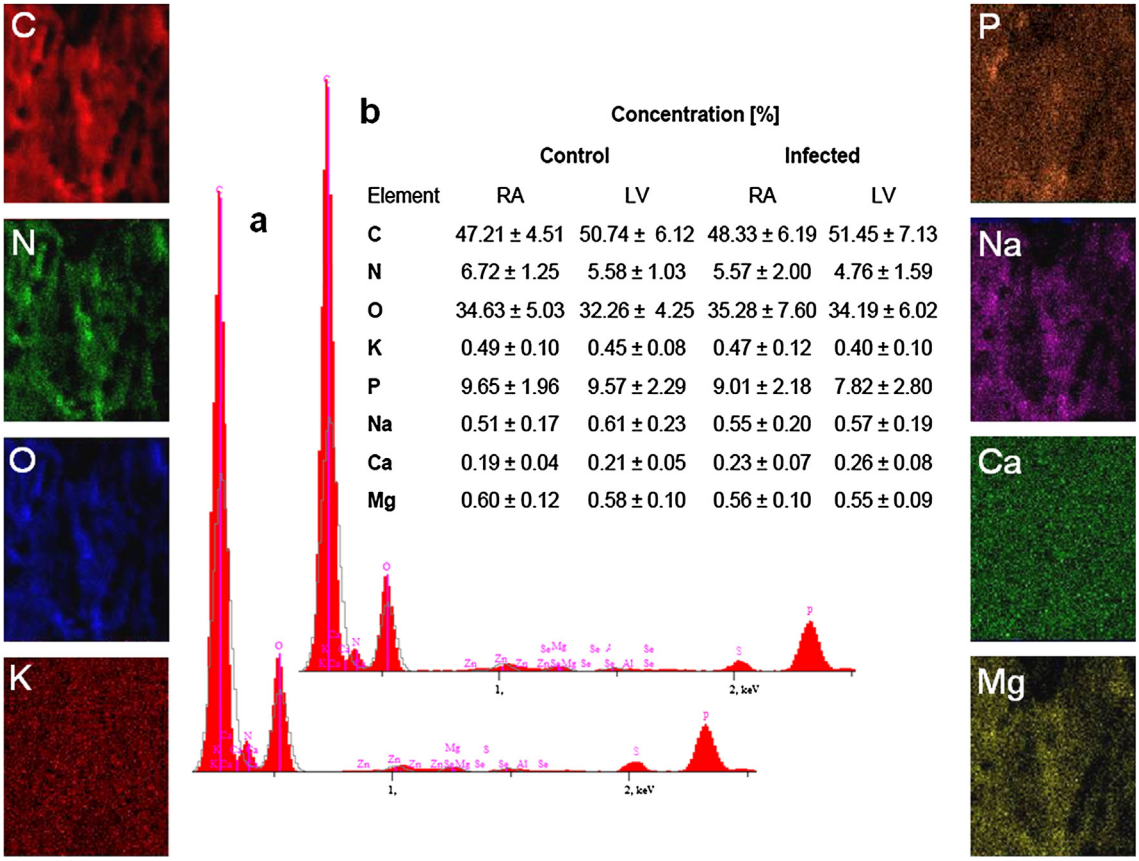

Fig. 6. Mineral content in the RA and LV of control and infected rats. The images in the left and right columns represent the mineral distribution map in the LV from control animals. In some images can be seen a cardiomyocyte profile. A representative spectrum of Energy Dispersive X-ray Spectroscopy is shown for each mineral in the LV from control (a) and infected (b) animals. The numbers (mean±S.D.) represent the proportion of minerals in the RA and LV for both groups. *There was no significant difference in the mineral proportion for each cardiac segment between the groups ($P>.05$), Student's t test.

interestingly, LV cardiomyocytes from IG animals had higher contractile amplitudes compared to the RA cardiomyocytes, suggesting a possible relationship between tissue vascularization and cardiomyocyte mechanical function. The presence of microvascular damage, such as thrombosis, vascular constriction and collapse, necrosis and derangement of the myocardial vascular network, is not unusual in ChC [6,11,29,31]. There is evidence that the reduction in myocardial vascularization constitutes an important component

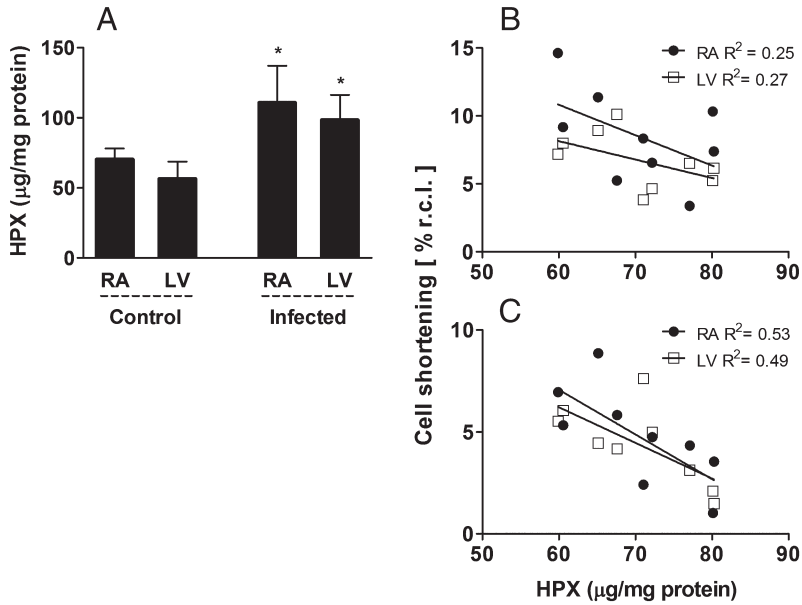

Fig. 7. Tissue levels of lipid HPX and correlations between HPX and cell shortening in the RA and LV from control (B) and infected (C) rats. In (A), the data are represented as mean±S.D. In (B) and (C), the mean of cell shortening per animal was plotted against the HPX levels in each cardiac segment for both groups. Shortening is expressed as % of resting cell length (% r.c.l.). *Denotes statistical difference from the control ($P<.001$) for the same segment, Student's t test.

involved in the deterioration of cardiac function in ChC [3,31]. Thus, the occurrence of an abnormal heart rhythm with the onset of electrical abnormalities such as complex arrhythmias and cardiac pump dysfunction are serious consequences of the myocardial hypoperfusion that decreases the mechanical efficiency of the heart [32,33]. These findings point to the close association between the cell and the ECM, in which complex and synergic relationships are indispensable to the maintenance of cardiac homeostasis [34–36]. There is sufficient evidence that different components of the ECM modulate several signaling pathways to control and maintain cardiac metabolism, growth, cellular, and muscular contractile performance, and rhythmicity [35–37]. Thus, the ECM creates a complex and finely tuned balance of cell interactions with the immediate environment. However, differences in the set point of this balance induced by regional or global pathological changes of the ECM result in substantial adaptations to the functional phenotype of cardiomyocytes, resulting in different spectra of cardiac dysfunction [34–36].

Considering the integration of cardiomyocytes with the ECM, it is not unrealistic to assume that the structural pathological remodeling of the myocardium induced by *T. cruzi* infection could potentially modify the molecular characteristics and physical properties of the ECM and subsequently impair the mechanisms that regulate the cellular contractile behavior, including mechanotransduction [34,37]. However, several aspects of the cellular and molecular basis of these changes remain to be clarified and require further investigation. On the other hand, the relationship between cardiac structure, cellular function and heart function, indicates that the pathological RA and LV myocardial remodeling observed in ChC may have several negative consequences, such as hypertrophy, and hemodynamic, electrical, and mechanical cardiac dysfunction [1–4,12,38]. Thus, cardiomyocitolysis and tissue necrosis with progressive destruction and subsequent reconfiguration of the heart parenchyma and stroma can be associated with a reduction in the contractile force and cardiac stroke volume [6,13,15,36]. The myocardial mechanical insufficiency is exacerbated by the extensive fibrosis that decreases the cardiac compliance and consequently decreases the efficiency of the frank-starling mechanism. This mechanism is essential for the modulation of cellular and muscular contraction forces [31,39], especially in conditions of autonomic denervation that are frequently seen in ChC [6,11,13]. Moreover, the abnormal organization pattern of collagen fibers may decrease the contractile efficiency of the heart since part of the force used for pumping blood is diverted to correct the geometric distortion determined by the structural disorganization of collagen and possibly cardiomyocytes [38].

Previous studies have identified an important regulatory role of the ECM in the distribution of water and electrolytes in cardiac tissue, which can be markedly impaired in cardiomyopathies, especially when associated with tissue necrosis [40,41]. Moreover, it is widely recognized that tissue electrolyte concentrations, especially of calcium, sodium and potassium, modulate the cell membrane excitability and are critical for proper cardiomyocyte and whole heart contractile performance [41,42]. Despite the intense pathological remodeling of the ECM, the minerals investigated in the RA and LV were distributed in similar proportions in both groups, a finding that reduced the influence of a possible tissue electrolytic imbalance on the results of cell contractility.

It has been systematically shown that reactive oxygen species (ROS) have potent effects on cardiomyocytes and the ECM. ROS can lead to irreversible cell damage or death, and can stimulate cardiac fibroblast proliferation, matrix metalloproteinase synthesis, ECM remodeling and fibrosis [8,43]. Increased ROS production, including that by lipid hydroperoxides, has been involved in the progression of cardiac dysfunction observed in heart diseases with different etiologies, such as diabetes mellitus, hypertension [43], and *T. cruzi* infection [7,8,10]. Growing evidence highlights ROS as important inducers of cardiomyocyte contractile dysfunction [10,44,45]. The increased HPX levels in the RA and LV of IG animals and the inverse and moderate correlation between cell shortening and HPX levels corroborate these findings, suggesting a possible participation of lipid peroxidation in the pathogenesis of the myocardial structural remodeling and the mechanical dysfunction of cardiomyocyte in ChC. The relationship between oxidative stress and cardiomyocyte mechanical insufficiency has been suggested since ROS directly influence contractile function by modifying proteins that modulate the excitation-contraction coupling. This includes the modification of thiol radicals on the ryanodine receptor, the suppression of L-type calcium channel currents and the oxidative inhibition of sarcoplasmic reticular Ca^{2+} ATPase and Ca^{2+} uptake [44,45]. Moreover, previous studies showed that *T. cruzi* infection stimulates the production of free radicals and causes a dysfunction in the cellular metabolism of energy via the uncoupling of several enzymatic complexes that are integrated with the electron transport chain [7–9]. However, the relationship of these molecular changes with myocardial structural remodeling and the cellular mechanics of *T. cruzi* infection are poorly understood and require further investigation.

In summary, the results indicate that *T. cruzi* infection induces global and pathological structural remodeling of the RA and LV myocardium. This remodeling does not influence the myocardial mineral concentration but coexists with cardiomyocyte contractility dysfunction, which was possibly related to a new and abnormal organization pattern of the myocardial stroma and the increased cellular lipid peroxidation.

Acknowledgments

The authors would like to acknowledge the "*Núcleo de Microscopia e Microanálise*" of the Federal University of Viçosa. Rômulo D. Novaes was a recipient of the PhD scholarship from CAPES. Antônio J. Natali and André Talvani are CNPq fellows.

References

[1] Santos FM, Lima WG, Gravel AS, Martins TA, Talvani A, Torres RM, et al. Cardiomyopathy prognosis after benznidazole treatment in chronic canine Chagas' disease. J Antimicrob Chemother 2012;67:1987-95.
[2] Lima MM, Rocha MO, Nunes MC, Sousa L, Costa HS, Alencar MC, et al. A randomized trial of the effects of exercise training in Chagas cardiomyopathy. Eur J Heart Fail 2010;12:866-73.
[3] Marin-Neto JA, Cunha-Neto E, Maciel BC, Simões MV. Pathogenesis of chronic Chagas' heart disease. Circulation 2007;115:1109-23.
[4] Rassi-Jr A, Rassi A, Marin-Neto JÁ. Chagas disease. Lancet 2010;375:1388-402.
[5] Guerri-Guttemberg RA, Grana DR, Ambrosio G, Milei J. Chagas cardiomyopathy: Europe is not spared! Eur Heart J 2008;29:2587-91.
[6] Rossi MA, Tanowitz HB, Malvestio LM, Celes MR, Campos EC, Blefari V, et al. Coronary microvascular disease in chronic Chagas cardiomyopathy including an overview on history, pathology, and other proposed pathogenic mechanisms. PLoS Negl Trop Dis 2010;4:1–12.
[7] Wen J, Garg N. Oxidative modification of mitochondrial respiratory complexes in response to the stress of *Trypanosoma cruzi* infection. Free Radic Biol Med 2004;37:2072-81.
[8] Wen J, Dhiman M, Whorton EB, Garg NJ. Tissue-specific oxidative imbalance and mitochondrial dysfunction during *Trypanosoma cruzi* infection in mice. Microbes Infect 2008;10:1201-9.
[9] Gupta S, Bhatia V, Wen JJ, Wu Y, Huang MH, Garg NJ. *Trypanosoma cruzi* infection disturbs mitochondrial membrane potential and ROS production rate in cardiomyocytes. Free Radic Biol Med 2009;47:1414-21.
[10] Gupta S, Wen J, Garg NJ. Oxidative stress in Chagas disease. Interdiscip Perspect Infect Dis 2009;1:1-8 [ID190354].
[11] Biolo A, Ribeiro AL, Clausell N. Chagas cardiomyopathy-where do we stand after a hundred years? Prog Cardiovasc Dis 2010;52:300-16.
[12] Lima MM, Nunes MC, Rocha MO, Beloti FR, Alencar MC, Ribeiro AL. Left ventricular diastolic function and exercise capacity in patients with Chagas cardiomyopathy. Echocardiography 2010;27:519-24.
[13] Morris SA, Tanowitz HB, Wittner M, Bilezikian JP. Pathophysiological insights into the cardiomyopathy of Chagas' disease. Circulation 1990;82:1900-9.
[14] Higuchi ML, Brito T, Reis MM, Barbosa A, Bellotti G, Pereira-Barreto AC, et al. Correlation between *Trypanosoma cruzi* parasitism and myocardial inflammatory infiltrate in human chronic chagasic myocarditis: light microscopy and immunohistochemical findings. Cardiovasc Path 1993;2:101-6.

[15] Rossi MA. Fibrosis and inflammatory cells in human chronic chagasic myocarditis: scanning electron microscopy and immunohistochemical observations. Int J Cardiol 1998;66:183-94.
[16] Martinelli PM, Camargos ERS, Azevedo AA, Chiari E, Morel G, Machado CRS. Cardiac NGF and GDNF expression during *Trypanosoma cruzi* infection in rats. Auton Neurosci 2006;130:32-40.
[17] Brener Z. Therapeutic activity and criterion of cure on mice experimentally infected with *Trypanosoma cruzi*. Rev Inst Med Trop São Paulo 1962;4:389-96.
[18] Cruz-Orive LM, Weibel ER. Recent stereological methods for cell biology: a brief survey. Am J Physiol 1990;25:8148-56.
[19] Scherle W. A simple method for volumetry of organs in quantitative stereology. Mikroskopie 1970;26:57-63.
[20] Mandarim-de-Lacerda CA. Stereological tools in biomedical research. An Acad Braz Sci 2003;75:469-86.
[21] Dorph-Petersen KA, Nyengaard JR, Gundersen HJ. Tissue shrinkage and unbiased stereological estimation of particle number and size. J Microsc 2001;204:232-46.
[22] Brüel A, Oxlund H, Nyengaard JR. The total length of myocytes and capillaries, and total number of myocyte nuclei in the rat heart are time dependently increased by growth hormone. Growth Horm IGF Res 2005;15:256-64.
[23] Junqueira LCU, Bignolas G, Brentani RR. Picrosirius staining plus polarization microscopy, a specific method for collagen detection in tissue sections. Histochem J 1979;11:447-55.
[24] Gundersen HJ, Bendtsen TF, Korbo L, Marcussen N, Moller A, Nielsen K, et al. Some new, simple and efficient stereological methods and their use in pathological research and diagnosis. APMIS 1988;96:379-94.
[25] Natali AJ, Wilson LA, Peckham M, Turner DL, Harrison SM, White E. Different regional effects of voluntary exercise on the mechanical and electrical properties of rat ventricular myocytes. J Physiol 2002;541:863-75.
[26] Roman-Campos D, Duarte HLL, Sales-Jr PA, Natali AJ, Ropert C, Gazzinelli RT, et al. Changes in cellular contractility and cytokines profile during *Trypanosoma cruzi* infection in mice. Basic Res Cardiol 2009;104:238-46.
[27] Nourooz-Zadeh J, Tajaddini-Sarmadi J, Wolf SP. Measurement of plasma hydroperoxide concentrations by the ferrous oxidation-xilenol orange assay in conjunction with thiphenylphosphine. Anal Biochem 1994;220:403-9.
[28] Bradford M. A rapid and sensitive method for quantitation of microgram quantities of protein utilizing the principle of protein-dye-binding. Anal Biochem 1976;72:248-54.
[29] Novaes RD, Penitente AR, Gonçalves RV, Talvani A, Neves CA, Maldonado IR, et al. Effects of *Trypanosoma cruzi* infection on myocardial morphology, single cardiomyocyte contractile function and exercise tolerance in rats. Int J Exp Pathol 2011;92:299-307.
[30] Novaes RD, Penitente AR, Talvani A, Natali AJ, Neves CA, Maldonado IRSC. Use of fluorescence in a modified dissector method to estimate the number of myocytes in cardiac tissue. Arq Bras Cardiol 2012;98:252-8.
[31] Higuchi ML, Fukasawa S, Brito T, Parzianello LC, Bellotti G, Ramires JAF. Different microcirculatory and interstitial matrix patterns in idiopathic dilated cardiomyopathy and Chagas' disease: a three dimensional confocal microscopy study. Heart 1999;82:279-85.
[32] Verani MS, Hartung GH, Hoepfel-Harris J, Welton DE, Pratt CM, Miller RR. Effects of exercise training on left ventricular performance and myocardial perfusion in patients with coronary artery disease. Am J Cardiol 1981;47:797-803.
[33] Meiler SEL, Ashton JJ, Moeschberger ML, Unverferth DV, Leier CV. An analysis of the determinants of exercise performance in congestive heart failure. Am Heart J 1987;113:1207-17.
[34] Ingber DE. Mechanical signaling and the cellular response to extracellular matrix in angiogenesis and cardiovascular physiology. Circ Res 2002;91:877-87.
[35] Brutsaert DL. Cardiac endothelial-myocardial signaling: its role in cardiac growth, contractile performance, and rhythmicity. Physiol Rev 2003;83:59–115.
[36] Kresh JY, Chopra A. Intercellular and extracellular mechanotransduction in cardiac myocytes. Pflugers Arch 2011;462:75-87.
[37] Parker KK, Ingber DE. Extracellular matrix, mechanotransduction and structural hierarchies in heart tissue engineering. Phil Trans R Soc B 2007;362:1267-79.
[38] Mady C, Ianni BM, Arteaga E, Montes GS, Caldini EG, Andrade G, et al. Relation between interstitial myocardial collagen and the degree of clinical impairment in Chagas' disease. Am J Cardiol 1999;84:354-6.
[39] Kitzman DW, Higginbotham MB, Cobb FR, Sheikh KH, Sullivan MJ. Exercise intolerance in patients with heart failure and preserved left ventricular systolic function: failure of the Frank-Starling mechanism. J Am Coll Cardiol 1991;17:1065-72.
[40] Lehr D. Tissue electrolyte alteration in disseminated myocardial necrosis. Ann N Y Acad Sci 1969;156:344-78.
[41] Toda N. Effects of calcium, sodium and potassium ions on contractility of isolated atria and their responses to noradrenaline. Br J Pharmacol 1969;36:350-67.
[42] Bers DM. Cardiac excitation–contraction coupling. Nature 2001;415:198-205.
[43] Dhalla NS, Temsah R, Netticadan T. Role of oxidative stress in cardiovascular diseases. J Hypertens 2000;18:655-73.
[44] Xu KY, Zweier JL, Becker LC. Hydroxyl radical inhibits sarcoplasmic reticulum Ca^{2+}-ATPase function by direct attack on the ATP binding site. Circulation Res 1997;80:76-81.
[45] Kaplan P, Babusikova E, Lehotsky J, Dobrota D. Free radical-induced protein modification and inhibition of Ca^{2+}-ATPase of cardiac sarcoplasmic reticulum. Mol Cell Biochem 2003;248:41-7.